Supporting Information

Core-shell Fe-N-C nanocatalyst with ultrathin porous carbon shell as a robust electrocatalyst for oxygen reduction reaction

Bin Yue[a], Kang Yang[a], Huaming Xie[a], Ying Lei*[a], Jianying Li[a], Yujun Si[b]

[a]*College of Chemical Engineering, Sichuan University of Science and Engineering, Zigong 643000, PR China*

[b]*College of Chemistry and Environmental Engineering, Sichuan University of Science and Engineering, Zigong 643000, PR China*

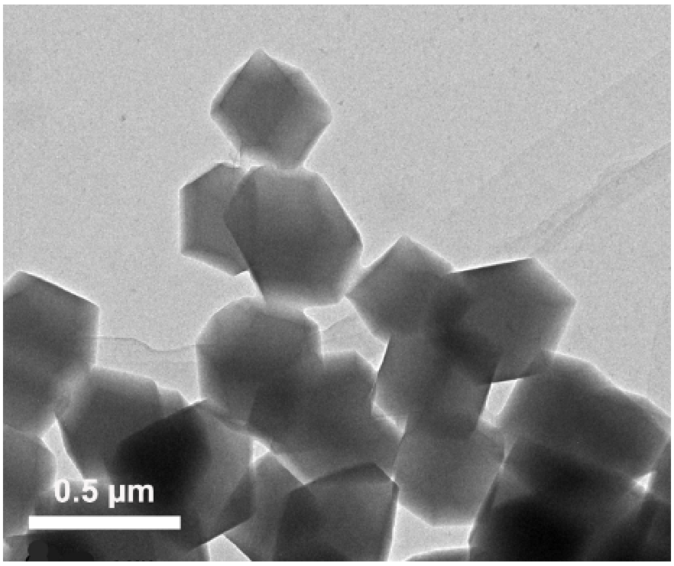

Figure. S1 TEM image of Fe-ZIF-8@PVP

Table S1. Pore structure characteristics of Fe-N-C@NC and Fe-N-C

Sample	surface area (m^2 g^{-1})	pore volume (cm^3 g^{-1})	pore diameter (nm)
Fe-N-C@NC	1163.9619	1.1459	3.9379
Fe-N-C	579.2399	0.9750	6.7330

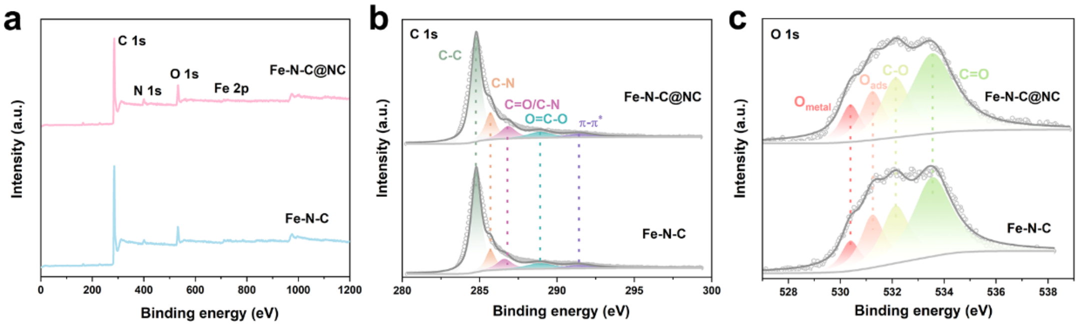

Figure. S2 High-resolution XPS spectra of (a) survey, (b) C 1s and (c) O 1s for Fe-N-C@NC and Fe-N-C.

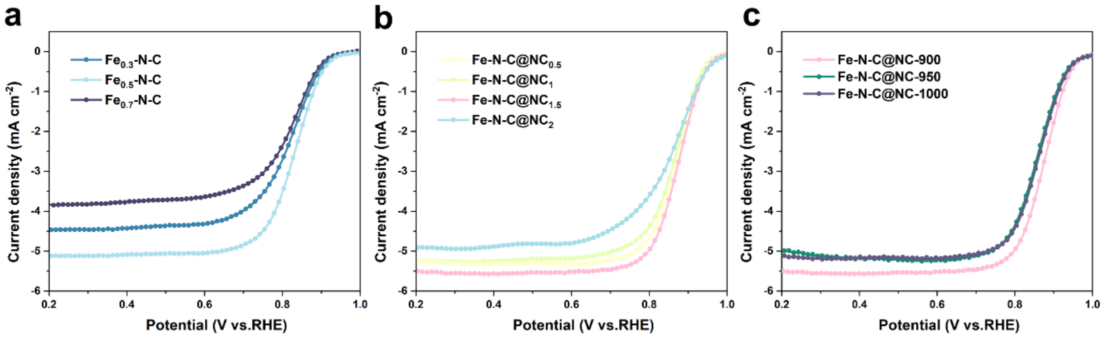

Figure. S3 (a) LSV curves of Fe-N-C with different molar of metallic iron (0.3 mmol, 0.5mmol and 0.7 mmol), (b) LSV curves of Fe-N-C@NC with different grams of polyvinylpyrrolidone (0.5g, 1g, 1.5g, 2g, with optimal metallic iron additions) and (c) LSV curves of Fe-N-C@NC with different pyrolysis temperatures (900 ^{o}C, 950 ^{o}C and 1000 ^{o}C)

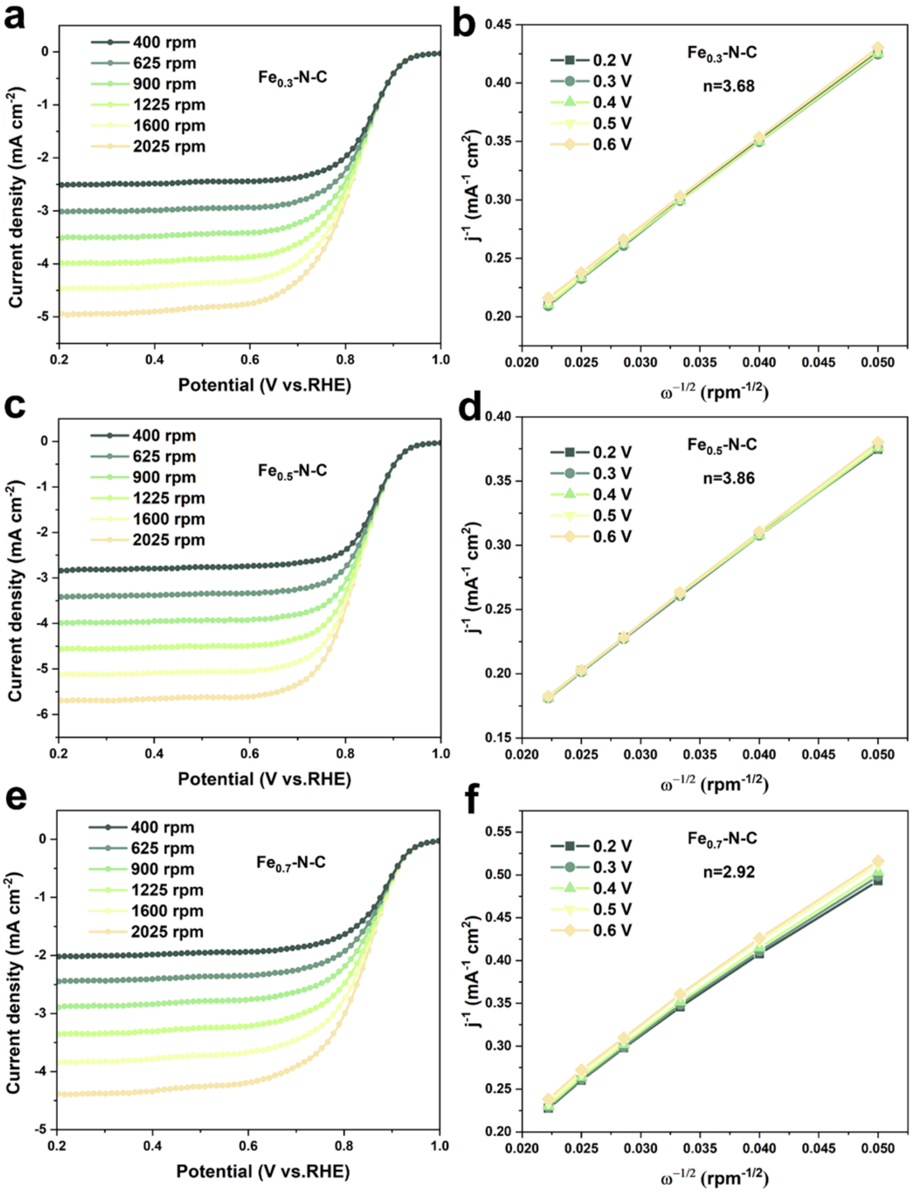

Figure. S4 LSV curves at various rotation rates for the ORR and the corresponding K-L plots for (a, b) $Fe_{0.3}$-N-C, (c, d) $Fe_{0.5}$-N-C, and (e, f) $Fe_{0.7}$-N-C in the O_2-saturated 0.1 M KOH solution, respectively.

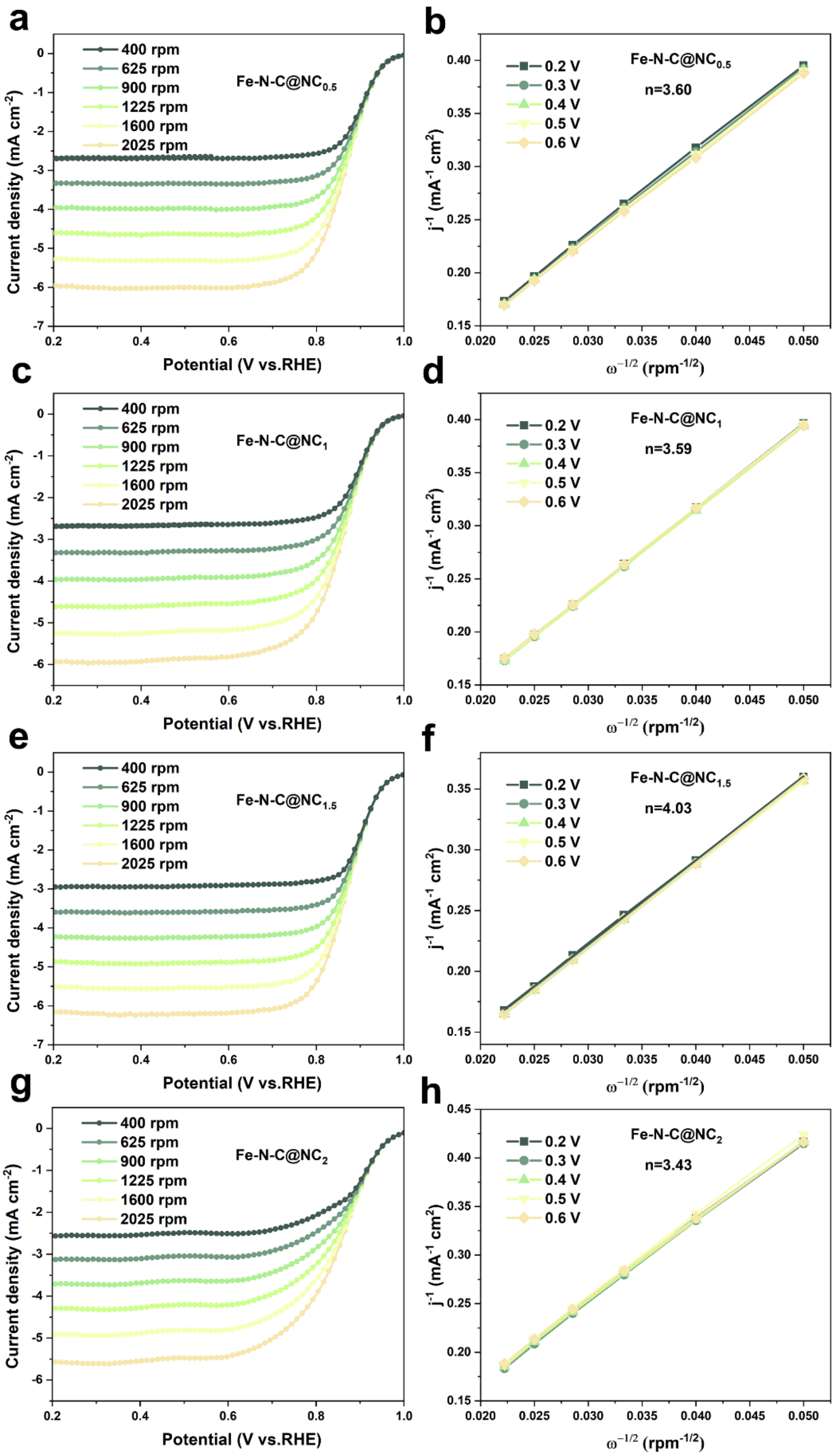

Figure. S5 LSV curves at various rotation rates for the ORR and the corresponding K-L plots for (a, b) Fe-N-C@$NC_{0.5}$, (c, d) Fe-N-C@NC_1, (e, f) Fe-N-C@$NC_{1.5}$, and (g, h) Fe-N-C@NC_2 in the O_2-saturated 0.1 M KOH solution, respectively.

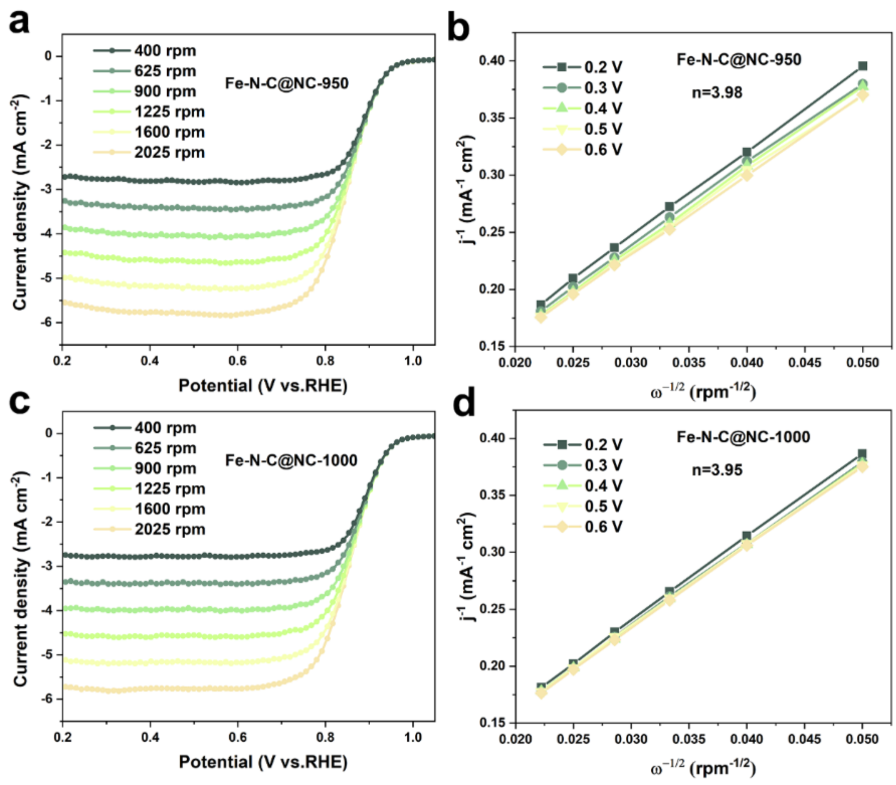

Figure. S6 LSV curves at various rotation rates for the ORR and the corresponding K-L plots for (a, b) Fe-N-C@NC-950 and (c, d) Fe-N-C@NC-1000 in the O_2-saturated 0.1 M KOH solution, respectively

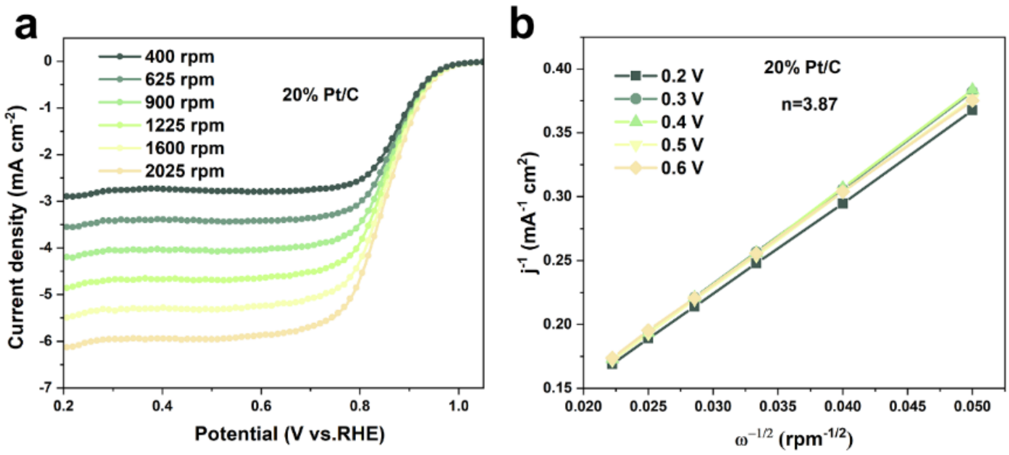

Figure. S7 LSV curves at various rotation rates for the ORR and the corresponding K-L plots for 20% Pt/C in the O_2-saturated 0.1 M KOH solution.

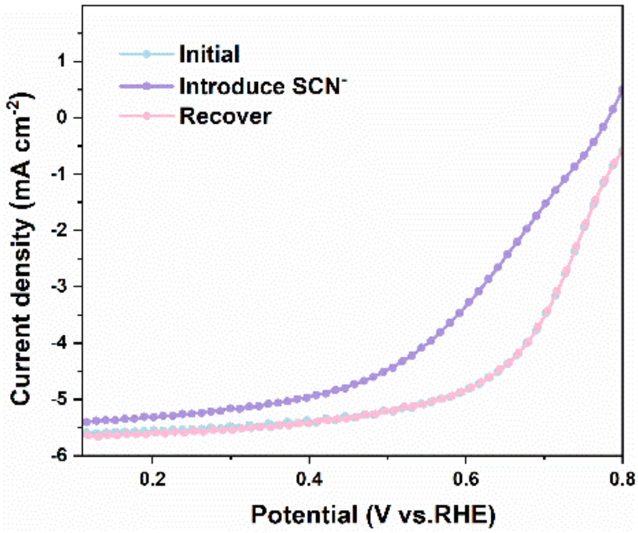

Figure. S8 LSV curves of Fe-N-C@NC before and after adding 5 mM NaSCN into 0.05M H_2SO_4. Electrode rotation speed, 1600 rpm; scan rate, 10 mV/s.

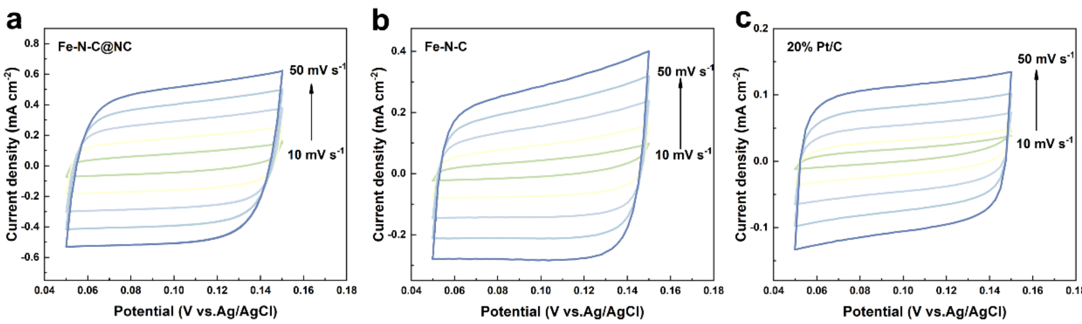

Figure. S9 CV at scan rates of 10, 20, 30, 40 and 50 mV s^{-1} in 0.1 M KOH electrolyte for (a) Fe-N-C@NC, (b) Fe-N-C and (c) 20% Pt/C.

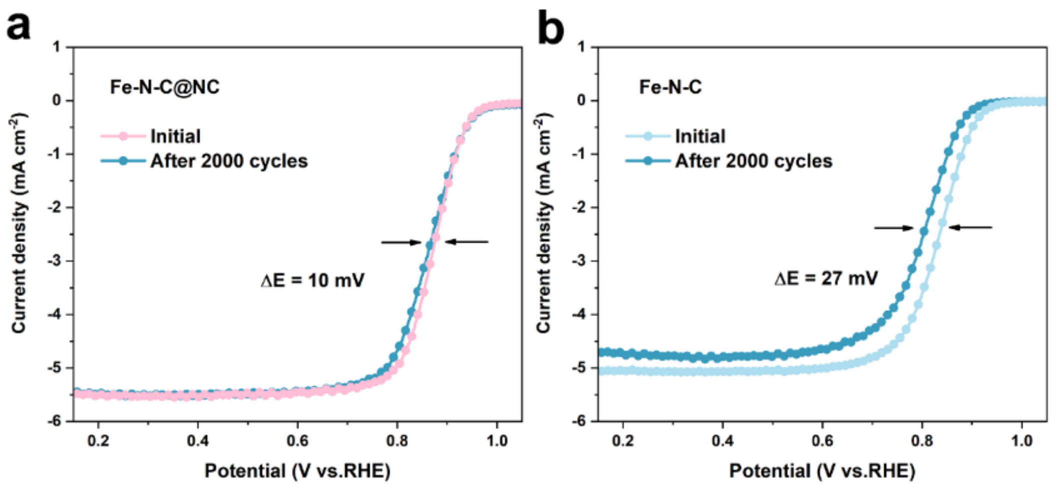

Figure. S10 LSV curves of Fe-N-C@NC and Fe-N-C after ADT.

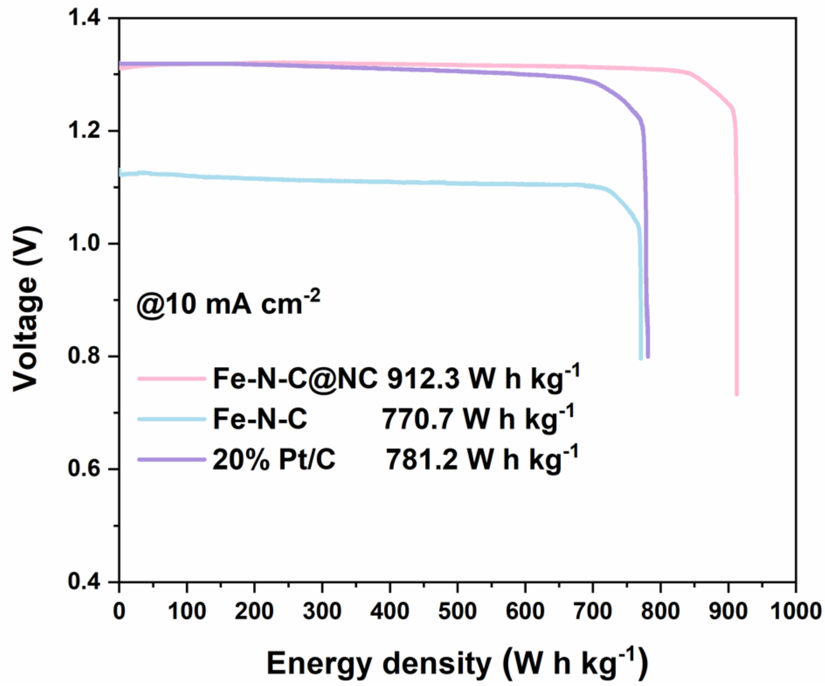

Figure. S11 voltage-energy density curves for different current densities.

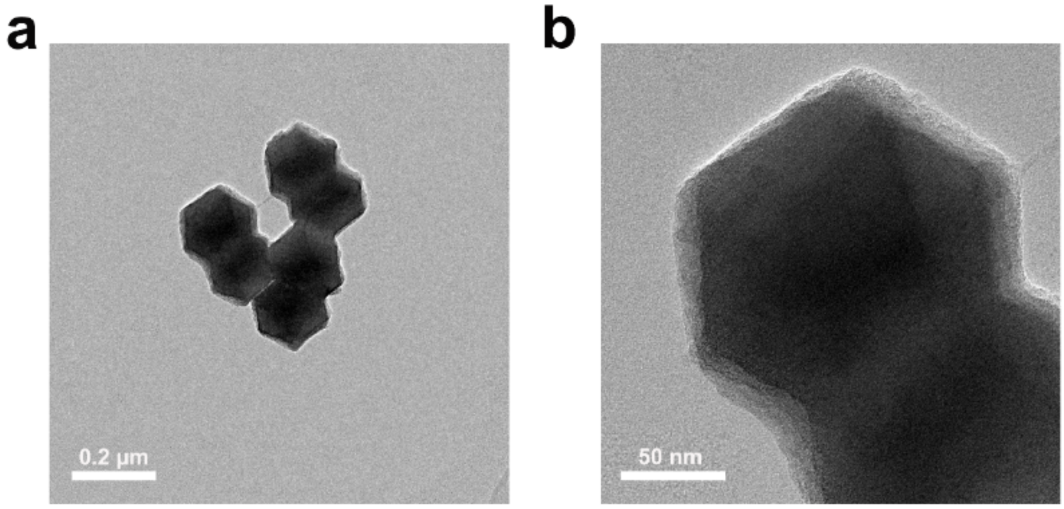

Figure. S12 TEM was used to test the Fe-N-C@NC material after cycling, and it was found that its morphology and structure were well preserved.

Table S2 Elemental analysis parameters of samples

Sample		C (at%)	N (at%)	O (at%)	Fe (at%)
Fe-N-C@NC	initial	80.87	3.27	14.65	1.21
	after 150 h	79.97	0.65	18.35	1.03
Fe-N-C	initial	80.54	2.97	14.44	2.05
	after 150 h	74.94	0.64	24.24	0.18

Table S3 Electrochemical performance of Zn-air batteries with our catalysts and other advanced catalysts reported recently.

Catalyst	Catalyst loading (mg cm^{-2})	Peak power density (mW cm^{-2})	Cycling time (h)	Reference
Fe-N-C@NC	1.0	170.8	150	This work
FeS/Fe_3C@NS-C-900	1.25	90.9	865	1
CeO_2-FeNC-5	4.0	169	200	2
Fe-N-C/2rGO	1.0	164	30	3
FeNC-0.04	1.0	165	-	4
NiFe(1:2)P/Pi	2.0	395	100	5
Fe-KJB-3-60A	0.15	251	156	6
Co SAs@PNCN	1.0	220	89	7
Fe-N/S-HPC	1.0	188.4	240	8
Fe/Co/Zn-CNZIF	-	156.7	137	9

Reference

1. Y. W. Li, W. J. Zhang, J. Li, H. Y. Ma, H. M. Du, D. C. Li, S. N. Wang, J. S. Zhao, J. M. Dou and L. Xu, Fe-MOF-Derived Efficient ORR/OER Bifunctional Electrocatalyst for Rechargeable Zinc-Air Batteries, ACS Appl. Mater. Interfaces, 2020, **40**, 44710-44719.
2. Y. Huang, Y. Zhang, J. Hao, Y. Wang, J. Yu, Y. Liu, Z. Tian, T. S. Chan, M. Liu, W. Li and J. Li, Tuning the coordination environment of Fe atoms enables 3D porous Fe/N-doped carbons as bifunctional electrocatalyst for rechargeable zinc-air battery, J. Colloid Interface Sci., 2022, **628**, 1067-1076.
3. X. Zhao, L. Shao, Z. Wang, H. Chen, H. Yang and L. Zeng, In situ atomically dispersed Fe doped metal-organic framework on reduced graphene oxide as bifunctional electrocatalyst for Zn-air batteries, J. Mater. Chem. C, 2021, **34**, 11252-11260.
4. Z. Meng, N. Chen, S. Cai, J. Wu, R. Wang, T. Tian and H. Tang, Rational design of hierarchically porous Fe-N-doped carbon as efficient electrocatalyst for oxygen reduction reaction and Zn-air batteries, Nano Res., 2021, **12**, 4768-4775.
5. N. Thakur, M. Kumar, D. Mandal and T. C. Nagaiah, Nickel Iron Phosphide/Phosphate as an Oxygen Bifunctional Electrocatalyst for High-Power-Density Rechargeable Zn-Air Batteries, ACS Appl. Mater. Interfaces, 2021, **44**, 52487-52497.
6. M. Wang, B. Huang, N. Jiang, T. Liu, J. Huang and L. Guan, An Fe-N-C electrocatalyst with dense active sites synthesized by expeditious pyrolysis of a natural Fe-N_4 macrocyclic complex, J. Mater. Chem. A, 2022, **43**, 23001-23007.
7. M. Zhang, H. Li, J. Chen, F. X. Ma, L. Zhen, Z. Wen and C. Y. Xu, Transition Metal (Co, Ni, Fe, Cu) Single-Atom Catalysts Anchored on 3D Nitrogen-Doped Porous Carbon Nanosheets as Efficient Oxygen Reduction Electrocatalysts for Zn-Air Battery, Small, 2022, **34**, 2202476.
8. M. Wang, X. Du, M. Zhang, K. Su and Z. Li, From S-rich polyphenylene sulfide to honeycomb-like porous carbon with ultrahigh specific surface area as bifunctional electrocatalysts for rechargeable Zn-air batteries, Carbon, 2022, **198**, 264-274.

9. Z. Guo, Y. Ma, Y. Zhao, Y. Song, S. Tang, Q. Wang and W. Li, Trimetallic ZIFs-derived porous carbon as bifunctional electrocatalyst for rechargeable Zn-air battery, J. Power Sources, 2022, **542**, 231723.